Research Article

Rapid Communications in Mass Spectrometry

Received: 4 July 2014 Revised: 22 August 2014 Accepted: 3 September 2014 Published online in Wiley Online Library

Rapid Commun. Mass Spectrom. **2014**, *28*, 2490–2496
(wileyonlinelibrary.com) DOI: 10.1002/rcm.7043

Laser ablation atmospheric pressure photoionization mass spectrometry imaging of phytochemicals from sage leaves

Anu Vaikkinen[1], Bindesh Shrestha[2], Juha Koivisto[3], Risto Kostiainen[1], Akos Vertes[2] and Tiina J. Kauppila[1]***

[1]Division of Pharmaceutical Chemistry and Technology, Faculty of Pharmacy, P.O. Box 56 (Viikinkaari 5 E), 00014 University of Helsinki, Helsinki, Finland
[2]Department of Chemistry, W.M. Keck Institute for Proteomics Technology and Applications, George Washington University, Washington, DC 20052, USA
[3]Department of Physics and Astronomy, University of Pennsylvania, 3231 Walnut Street, Philadelphia, PA 19104, USA

RATIONALE: Despite fast advances in ambient mass spectrometry imaging (MSI), the study of neutral and nonpolar compounds directly from biological matrices remains challenging. In this contribution, we explore the feasibility of laser ablation atmospheric pressure photoionization (LAAPPI) for MSI of phytochemicals in sage (*Salvia officinalis*) leaves.
METHODS: Sage leaves were studied by LAAPPI-time-of-flight (TOF)-MSI without any sample preparation. Leaf mass spectra were also recorded with laser ablation electrospray ionization (LAESI) mass spectrometry and the spectra were compared with those obtained by LAAPPI.
RESULTS: Direct probing of the plant tissue by LAAPPI efficiently produced ions from plant metabolites, including neutral and nonpolar terpenes that do not have polar functional groups, as well as oxygenated terpene derivatives. Monoterpenes and monoterpenoids could also be studied from sage by LAESI, but only LAAPPI was able to detect larger nonpolar compounds, such as sesquiterpenes and triterpenoid derivatives, from the leaf matrix. Alternative MSI methods for nonpolar compounds, such as desorption atmospheric pressure photoionization (DAPPI), do not achieve as good spatial resolution as LAAPPI (<400 μm).
CONCLUSIONS: We show that MSI with LAAPPI is a useful tool for concurrently studying the distribution of polar and nonpolar compounds, such as phytochemicals, directly from complex biological samples, and it can provide information that is not available by other, established methods.

Mass spectrometry imaging (MSI) is a method for studying the spatial distributions of molecules or atoms on and below sample surfaces.[1–3] It provides a unique view of molecular composition at spatial resolution that is difficult to attain with traditional methods. In biochemistry and medicine, MSI is a valuable tool for the study of, e.g., disease markers,[4] single cells,[5] and subcellular structures.[6] Typical techniques used in MSI include matrix-assisted laser desorption/ionization (MALDI),[7] secondary ion mass spectrometry (SIMS),[8] desorption electrospray ionization (DESI),[9,10] and laser ablation electrospray ionization (LAESI).[11]

Here, we explore the feasibility of a recently introduced ambient ionization technique, laser ablation atmospheric pressure photoionization (LAAPPI),[12] for MSI. For microsampling, LAAPPI uses a mid-infrared (mid-IR) laser at 2.94 μm wavelength to ablate the sample through the excitation of its endogenous water.[13,14] The ejected sample material is then desolvated with a hot jet of solvent vapour. A krypton discharge lamp that produces 10.0 and 10.6 eV photons is used to irradiate the combined sample and solvent plumes to achieve photoionization of the solvent, and, subsequently, the sample molecules by gas-phase ion-molecule reactions. Because of the ionization mechanism,[12,15] LAAPPI is better suited for low polarity and nonpolar compounds than, e.g., LAESI, which shows high ionization efficiencies for ionic and polar compounds. Other ambient ionization methods, such as direct analysis in real time (DART)[16] and desorption atmospheric pressure photoionization (DAPPI),[17] are also suitable for the analysis of low polarity compounds, but typically exhibit limited spatial resolution (~3 mm[18] and ~1 mm,[19] respectively).

In this contribution, sage (*Salvia officinalis*) leaves were chosen as a tissue model. In addition to being used as a culinary herb, sage has been recognized to have potential anti-oxidant[20] and anti-inflammatory properties. The sage plant is known to excrete essential oil that is rich in low polarity terpenes and terpenoids. The bioactivity of sage has been associated with diterpenes, such as carnosic acid[21] and carnosol,[21] and can also be due to triterpenes, e.g., ursolic acid found

* *Correspondence to:* T. J. Kauppila, Division of Pharmaceutical Chemistry and Technology, Faculty of Pharmacy, University of Helsinki, P.O. Box 56 (Viikinkaari 5 E), 00014 University of Helsinki, Helsinki, Finland.
E-mail: tiina.kauppila@helsinki.fi
** *Correspondence to:* A. Vertes, Department of Chemistry, W.M. Keck Institute for Proteomics Technology and Applications, George Washington University, Washington DC 20052, USA.
E-mail: vertes@gwu.edu

Rapid Communications in Mass Spectrometry

in the plant leaves.[22,23] Here, we demonstrate the feasibility of LAAPPI-MS to image such low polarity compounds directly from sage leaves.

EXPERIMENTAL

The sage (*Salvia officinalis*) twigs were obtained from a local supermarket and stored at ~4 °C before analysis. The leaves were detached from the stem a few minutes before the analysis, placed on glass microscope slides with the abaxial side exposed, and attached to the surface with adhesive tape.

An AccuTOF JMS-T100LC mass spectrometer (JEOL, Peabody, MA, USA) was used for mass analysis. The inlet cone (orifice) temperature was set to 150 °C and its voltage was kept at 20 V. The data acquisition time was selected as 1 s per scan. The base peak of the LAAPPI spectra at *m/z* 231.1, produced by the photooxidation of the anisole solvent jet with the formula $[C_{14}O_3H_{14}+H]^+$, was used for internal mass calibration. Similar photooxidation reactions have been previously described for benzene and toluene in atmospheric pressure photoionization.[24]

The commercial ion source of the mass spectrometer was replaced by a home-built LAAPPI source similar to one described in the literature (Fig. 1).[12] A mid-IR laser beam was delivered in front of the mass spectrometer inlet orifice using two gold-coated mirrors (PF10-03-M01; Thorlabs, Newton, MA, USA) and focused to the surface of a sample by an anti-reflection coated 50-mm focal length planoconvex CaF_2 lens (Thorlabs). The sample was placed on a microscope slide mounted on a Peltier cooling stage and positioned in front of the mass spectrometer ~10 mm below the inlet orifice. The temperature of the sample was kept at ~18 °C to minimize dehydration. The mid-IR laser beam was produced by an optical parametric oscillator that converted the 5 ns pulsed output of a Nd:YAG laser (Vibrant IR; Opotek, Carlsbad, CA, USA) to 2.94 μm wavelength at 10 Hz repetition rate. The energy was selected as ~2 mJ/pulse that, based on the area of the sampling spot, corresponded to a calculated fluence of ~1.3 J/cm^2. The ablation plume was intercepted by a hot anisole vapor jet that was directed toward the inlet of the mass spectrometer. The jet was produced using an all-glass heated nebulizer microchip

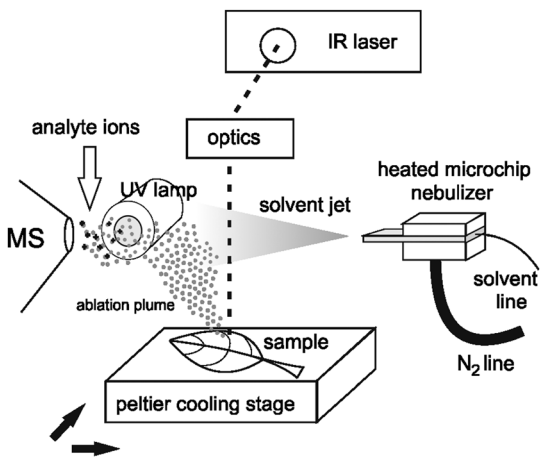

Figure 1. Schematic representation of the LAAPPI ion source and operational principle (not to scale).

described in detail previously.[25] The liquid solvent (anisole) was introduced into the microchip heater at 0.5 μL/min using a syringe pump (Physio 22; Harvard Apparatus, Holliston, MA, USA), and vaporized with the aid of nitrogen gas flow (100 mL/min) and high temperature (3.0 W heating power producing ~300 °C jet temperature). The mixture of sample plume and solvent jet was irradiated in the ambient air with 10.0 and 10.6 eV photons produced by a krypton discharge vacuum ultraviolet (VUV) photoionization lamp (PKR 100; Heraeus Noblelight, Cambridge, UK), leading to photoionization of the anisole molecules and subsequent gas-phase reactions resulting in the ionization of the analytes.

The leaves were rastered by moving the cooled Peltier stage in the xy-plane using a computer-controlled motorized xyz-stage (LTA-HS; Newport Corp., Irvine, CA, USA). A previously described LabVIEW-based controlling program[26] was used to operate the stage and to record the ablation spot position information in the experiments. The sampling step size was set to 400 μm and the dwell time was 5 s. The mass spectra and the time-resolved ion intensities (corresponding to extracted ion chromatograms (EICs)) were recorded using the native mass spectrometer software provided by the manufacturer of the instrument (JEOL). The individual EICs were exported as text files and combined with the time-resolved positioning information to produce the MS contour plot images by a home-written Python script. The data was also subjected to correlation and co-localization analysis. The Python script and correlation analysis methods are described in detail in the Supporting Information.

The LAESI data was obtained from a second sage plant using the same mass spectrometer and IR laser (10 Hz) as for LAAPPI, and a LAESI ion source similar to that described previously.[11] Briefly, the ESI solvent was 50% MeOH solution with 0.1% acetic acid at 500 nL/min flow rate (SP 100i; World Precision Instruments, Inc., Sarasota, FL, USA), and it was sprayed using a tapered stainless steel emitter (i.d. 50 μm, MT320-50-5-5; New Objective, Woburn, MA, USA) kept at +3300 V (PS350; Stanford Research Systems, Sunnyvale, CA, USA).

RESULTS AND DISCUSSION

A typical LAAPPI spectrum from a sage leaf is presented in Fig. 2(a). The spectra were searched for ions that could be related to bioactive sage phytocompounds (Table 1), well known from extensive studies of the chemical composition of sage leaves.[20,21,23,27–30] Because sage leaves express a high number of isobaric substances, the absolute identification of the observed ions is not possible without MS^n studies. Even if MS^n data was available, absolute structure elucidation would be cumbersome without applying either chromatographic or ion mobility separation and additional techniques, such as nuclear magnetic resonance (NMR), because of the almost identical fragmentation of some analytes, e.g., in the case of mono- and sesquiterpenes.

The observed peaks were thought to be due to $M^{+\cdot}$, MH^+, and $[M–H]^+$ type ions and/or fragments of the sage phytochemicals. The data suggest that LAAPPI-MSI is able to detect nonpolar hydrocarbons, such as mono- and sesquiterpenes ($M^{+\cdot}$ corresponding to *m/z* 136.14 and 204.20 ions, respectively), their oxygenated derivatives (e.g., keto and

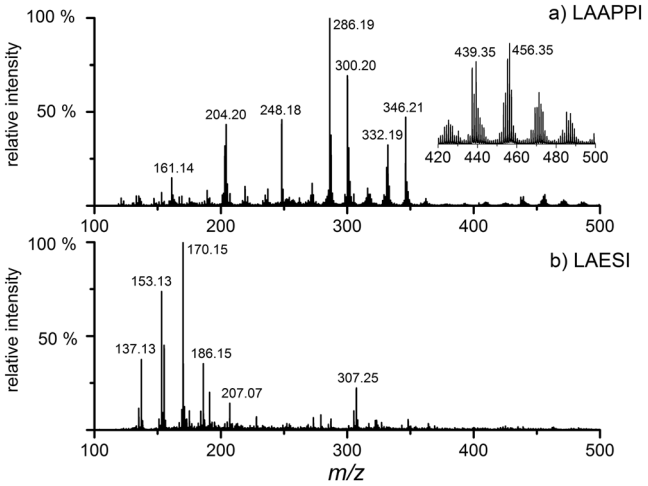

Figure 2. Typical (a) LAAPPI and (b) LAESI mass spectra from sage leaf. The solvent background has been subtracted and the intensities have been normalized to respective base peak intensities.

hydroxyl group containing monoterpenoids with MH^+ corresponding to the *m/z* 153.14 and 155.15 ions, respectively), as well as di- and triterpene derivatives, e.g., carnosic acid ($M^{+\cdot}$ corresponding to the *m/z* 332.19 ion), and ursolic and/or oleanolic acid ($M^{+\cdot}$ corresponding to the *m/z* 456.35 ion). Previously,[12,36] LAAPPI has been shown to be able to ionize similar neutral and nonpolar compounds such as cholesterol, dehydroisoandrosterone, cholecalciferol, alphatocopherol, and pyrene.

To compare LAAPPI with the more established laser ablation method LAESI, which utilizes electrospray for ionization, we also analyzed a sage leaf sample with LAESI (Fig. 2(b)). LAESI could detect monoterpenes and terpenoids showing MH^+ ions at *m/z* 137.13, 153.13, and 155.14, and possibly $[M+NH_4]^+$, $[M+Na]^+$ and $[M+K]^+$ ions of keto-group-containing monoterpenoids at *m/z* 170.15, 175.11, and 191.08, respectively. Ions at *m/z* 273.26 and 305.24 may be the dimers of the monoterpenes and hydroxyl-group-containing terpenoids, respectively. However, unlike LAAPPI, LAESI could not detect the larger terpenes and terpenoids. For example, the nonpolar sesquiterpenes ($M^{+\cdot}$ at *m/z* 204.20 in LAAPPI) and larger di- and triterpene derivatives were absent in the spectra. Thus, we conclude that LAAPPI is an attractive method to detect nonpolar compounds directly from tissue matrix.

The compounds observed by LAAPPI may also be studied using desorption atmospheric pressure chemical ionization (DAPCI), DART, or DAPPI, as oxygenated terpenes (e.g., camphor) have been analysed previously from camphor wood by DAPCI,[37] and both terpenes and terpenoids have been analyzed from eucalyptus by DART.[38] Although the ionization mechanisms of DAPPI and LAAPPI are similar, previously reported high-resolution DAPPI-MSI spectra of sage leaves[19] did not show mono- and sesquiterpene ions with as high abundances as obtained by LAAPPI here. The difference could be due to the age of the sample, as in the LAAPPI-MSI analysis fresh leaves were studied, whereas in DAPPI the leaves were dried before the analysis; thus, volatile low molecular weight analytes might have evaporated from the latter sample. The spatial resolutions of DART and DAPPI have been reported to be 3 and 1 mm, respectively,[18,19] and that of DAPCI can be expected to be of the same level, as also it uses heated gas for desorption. In this study, a 400-µm step size was used without an overlap of the adjacent spots, making LAAPPI-MS feasible for MSI. As can be seen from Fig. 3(b), the ultimate spatial resolution of LAAPPI in this configuration (defined by the size of the ablation crater) is, however, slightly lower, ~300 µm. While DESI does achieve similar or better (down to 35 µm) spatial resolution[10,39,40] than the LAAPPI experiments reported here, we expect the electrospray-based ionization mechanism to lead to similar spectra to LAESI.

Figures 3(a) and 3(b) show a photograph and a post-analysis microscope image of the studied sage leaf, respectively, and LAAPPI mass spectrometry images of the spatial distributions of selected ions from the target can be found in Figs. 3(c)–3(i). The ion intensity images of suspected mono- and sesquiterpene ions, $M^{+\cdot}$ at *m/z* 136.14 (Fig. 3(c)) and 204.20 (Fig. 3(g)), respectively, clearly reveal the location of the extended petiole (midrib), as these ions give a very low signal in that region compared with in other parts of the leaf. Sage leaves have been previously reported to contain 22-fold quantities of essential sage oil[29] and over 3-fold amounts of mono- and sesquiterpenes[30] compared with the stems that serve similar functions in the plant as the midrib. The lower overall ion abundance from the midrib can also be partly due to the higher tensile strength of the midrib tissue than of the cells of the lamina, resulting in a lower ablation efficiency of the former. As the width of the midrib is ~400 µm at the apex of the leaf, where it is clearly visible in some of the MS images (Fig. 3), the LAAPPI-MSI effective spatial resolution in this study can be estimated to be equal to the applied step size, i.e., 400 µm.

Further examination of the maps in Figs. 3(c)–3(i) shows that the ions at *m/z* 136.07 and 456.35 have very different spatial distributions from the ions at *m/z* 136.14 and 204.20. Literature comparison suggests that the ion at *m/z* 456.35 corresponds to the radical cation, $M^{+\cdot}$, of ursolic (or oleanolic) acid that has previously been associated with the epicuticular wax coating of the leaves of *Salvia blepharophylla*,[41] and wax coatings of many other plants and their fruits, such as apples. The MS image (Fig. 3(i)) implies that the wax crystals could be more abundant in the vicinity of the midrib and veins; however, the size of the ablated area and the pre-set laser fluence do not help to confirm this, because the width of the veins is below 300 µm. We expect that the spatial resolution and the sampling step size can be improved by the use of aspherical lenses or sharpened optical fibers that focus the ablating laser beam more tightly. This is likely to reduce the ion signal, which, however, is not a limiting factor in the analysis of many of the observed ions, but in the case of low abundance ions, such as that at *m/z* 456.35, the loss could be compensated for by improving ion collection efficiency.

Furthermore, the results imply that LAAPPI-MSI could be used to study the metabolism of terpenes and terpenoids. In sage, they are known to be synthesized from geranyl pyrophosphate.[35] Geranyl pyrophosphate is converted into different monoterpenes ($M^{+\cdot}$ corresponding to the *m/z* 136.14 ion) by sage pinene synthetases,[35] and into borneol (MH^+ corresponding to the *m/z* 155.15 ion), which oxidizes to camphor (MH^+ corresponding to the *m/z* 153.14 ion) by respective metabolic pathways.[42,43] Possible artifacts due to rapid VUV photon or air-induced oxidation were ruled out by correlation analysis: the ion distributions had a relatively weak correlations

Rapid Communications in Mass Spectrometry

Table 1. Selected ions observed in LAAPPI-MSI analysis and their tentative assignments based on previously reported phytochemicals of *Salvia officinalis* leaves (or sage cell cultures in Funk *et al.*;[32] compounds marked with*)

Observed *m/z*	CG	Reported phytochemicals of sage leaves with same *m/z*	Chemical formula	Calculated *m/z*	Δ*m/z*
121.112		N/A	$C_9H_{13}^+$	121.101	0.012
133.115	1	p-cymene[30,31] $[M–H]^+$	$C_{10}H_{13}^+$	133.101	0.014
135.128		p-cymene[30,31] MH^+	$C_{10}H_{15}^+$	135.117	0.011
		monoterpenes (e.g., α-pinene/β-pinene/ limonene/camphene)[29–31] $[M–H]^+$			
		monoterpenoids (e.g., camphor/α-thujone/ β-thujone)[29–31] $[MH–H_2O]^+$			
136.068		N/A	$C_8H_8O_2^{+\cdot}$	136.052	0.016
136.137		monoterpenes (e.g., α-pinene/β-pinene/ limonene/camphene)[29–31] $M^{+\cdot}$	$C_{10}H_{16}^{+\cdot}$	136.125	0.012
		monoterpenoids (e.g., borneol/1,8-cineole/ terpinen-4-ol)[29–31] $[M-H_2O]^{+\cdot}$			
147.132	2	N/A	$C_8H_{19}O_2^+$	147.138	−0.006
		N/A	$C_{11}H_{15}^+$	147.117	0.015
153.140		monoterpenoids (e.g., borneol/1,8-cineole/ terpinen-4-ol)[29–31] $[M–H]^+$	$C_{10}H_{17}O^+$	153.127	0.013
		monoterpenoids (e.g., camphor/α-thujone/ β-thujone/myrtenol)[29–31] MH^+			
155.152		monoterpenoids (e.g., borneol/1,8-cineole/ terpinen-4-ol)[29–31] MH^+	$C_{10}H_{19}O^+$	155.143	0.009
161.140		N/A	$C_{12}H_{17}^+$	161.132	0.008
167.119		6-oxocamphor[32]* MH^+	$C_{10}H_{15}O_2^+$	167.107	0.013
		6-hydroxycamphor[32]* $[M–H]^+$			
169.129		6-hydroxycamphor[32]* MH^+	$C_{10}H_{17}O_2^+$	169.122	0.007
175.152		N/A	$C_{13}H_{19}^+$	175.148	0.004
189.173	3	N/A	$C_{14}H_{21}^+$	189.164	0.009
203.187	1, 3	sesquiterpenes (e.g. α-humulene/β-caryophyllene)[29–31] $[M–H]^+$	$C_{15}H_{23}^+$	203.179	0.008
		caryophyllene oxide[29–31] $[MH–H_2O]^+$			
204.196	2	sesquiterpenes (e.g. α-humulene/β-caryophyllene)[29–31] $M^{+\cdot}$	$C_{15}H_{24}^{+\cdot}$	204.187	0.009
		viridiflorol[29–31] $[M–H_2O]^{+\cdot}$			
219.173	4	caryophyllene oxide[29–31] $[M–H]^+$	$C_{15}H_{23}O^+$	219.174	−0.001
		$[237.189–H_2O]^+$ **			
237.189	4	N/A	$C_{15}H_{25}O_2^+$	237.185	0.004
248.178	5	N/A	$C_{16}H_{24}O_2^{+\cdot}$	248.178	0.001
272.243		monoterpenes (e.g. α-pinene/β-pinene/ limonene/camphene)[29–31] $[2M]^{+\cdot}$	$C_{20}H_{32}^{+\cdot}$	272.250	−0.007
		manool[29–31] $[M–H_2O]^+$			
286.187	6	carnosol $[M–CO_2]^+$[21]***	$C_{19}H_{26}O_2^{+\cdot}$	286.193	−0.006
		carnosic acid $[M–CO–H_2O]^+$[21]***			
300.203	7	dehydroabietic acid[33] $M^{+\cdot}$	$C_{20}H_{28}O_2^{+\cdot}$	300.209	−0.006
		miltirone[34] $[M+NH_4]^+$	$C_{19}H_{26}O_2N^+$	300.196	0.007
315.077		geranyl pyrophosphate[35] MH^+	$C_{10}H_{21}O_7P_2^+$	315.076	0.001
316.198	7	hydroxydehydroabietic acid[33] $M^{+\cdot}$	$C_{20}H_{28}O_3^{+\cdot}$	316.203	0.005
331.190	6	carnosol[21] MH^+	$C_{20}H_{27}O_4^+$	331.190	0.000
		carnosic acid[21] $[M-H]^+$			
332.188	6	carnosic acid[21] $M^{+\cdot}$	$C_{20}H_{28}O_4^{+\cdot}$	332.199	−0.011
346.212	6	12-*O*-methyl carnosic acid[34] $M^{+\cdot}$	$C_{21}H_{30}O_4^{+\cdot}$	346.214	−0.002
437.341	5	ursolic acid/oleanolic acid[23] $[M–H–H_2O]^+$	$C_{30}H_{45}O_2^+$	437.341	0.000
439.353	5	ursolic acid/oleanolic acid[23] $[MH–H_2O]^+$	$C_{30}H_{47}O_2^+$	439.357	−0.004
455.345	5	ursolic acid/oleanolic acid[23] $[M–H]^+$	$C_{30}H_{47}O_3^+$	455.352	−0.007
456.352	5	ursolic acid/oleanolic acid[23] $M^{+\cdot}$	$C_{30}H_{48}O_3^{+\cdot}$	456.360	−0.008

CG (correlation group): shows strongly spatially correlated pairs and groups of ions. Strong correlation possibly indicates fragmentation or oxidation during ionization or exposure to air. Details of the correlation analysis are presented in the Supporting Information. N/A: not available. The ion marked with ** is a possible fragmentation product based on the observed *m/z*. The ions marked with *** have been reported previously in EI-MS spectra as fragments of carnosol and carnosic acid, respectively.[21]

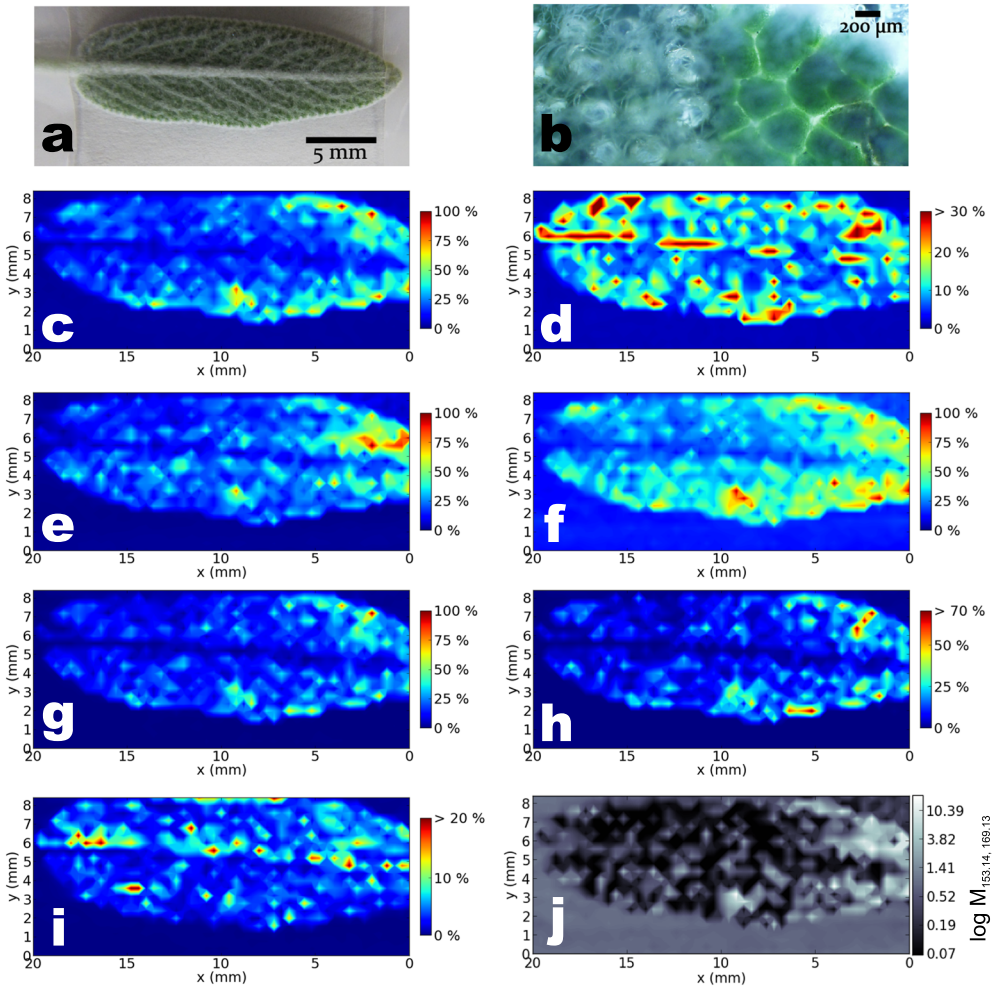

Figure 3. (a) Photograph of the sage leaf before analysis and (b) post-analysis microscope image of the analyzed sample near the apex. Mass spectrometry images showing the spatial distributions of ions at *m/z* (c) 136.14, (d) 136.07, (e) 153.14, (f) 169.13, (g) 204.20, (h) 332.19, and (i) 456.35 (normalized to the maximum intensity of each ion. Note that in (d), (h), and (i) the low intensity range was zoomed in for better visualization with an upper limit of 30, 70, and 20 %, respectively). (j) Pearson colocalization map of the ions at *m/z* 153.14 and 169.13 (note the logarithmic scale and see the Supporting Information for details). See Table 1 for previously identified sage phytochemicals possibly corresponding to the observed *m/z* values.

(r(*m/z* 136.14, 153.14) = 0.861 and r(*m/z* 136.14, 155.15) = 0.932, see Supporting Information), while much higher correlation was observed for pairs of ions linked by fragmentation (e.g., the putative oleanolic/ursolic acid $M^{+\cdot}$ ion at *m/z* 456.35, and the $[MH–H_2O]^+$ ion at *m/z* 439.35 had r = 0.986). Thus, the distributions probably reflect the local metabolism in the leaf. The location of the ions could reflect tissue aging, as, e.g., camphor is produced in young leaves and its amount increases as the leaf ages.[43] In addition, stress induced by water deficiency has been shown to increase monoterpene content in sage,[44] and, as the sample was obtained as twigs that had suffered at least several hours of water deficiency, stress-induced metabolism is likely to be detectable. In addition, more in-depth studies of leaves at different stages of senescence may provide a detailed view on the metabolic oxidation of camphor (MH^+ calculated *m/z* 153.13) to 6-hydroxycamphor (MH^+ calc. *m/z* 169.12) and further to 6-oxocamphor (MH^+ calc. *m/z* 167.11) and other metabolites known to form during leaf senescence.[32] Figure 3(j) shows that the *m/z* 153.14 and 169.13 ions are colocalized near the apical end of the studied leaf, where both ions also show highest abundances indicating that the highest metabolic activity is seen in this area.

CONCLUSIONS

We have demonstrated that LAAPPI can be applied to MSI of plant leaf tissues. LAAPPI enabled the analysis of typical hydrocarbon phytochemicals, such as mono- and sesquiterpenes as well as more polar terpene derivatives, in sage leaves. Only a limited sub-set of these compounds was detected by the electrospray-based LAESI-MS. In this experiment LAAPPI achieved roughly 400 µm spatial resolution, which is better than previously reported for nonpolar compounds in ambient MS. The study confirmed that LAAPPI can be used to explore the spatial distribution of nonpolar plant compounds typically analyzed by gas

Rapid Communications in Mass Spectrometry

chromatography (GC) and liquid chromatography (LC)/MS, and it is expected to become a useful tool for the study of nonpolar compounds from various tissues, thus complementing LAESI, DESI and MALDI in MSI.

Acknowledgements

Professor Heikki Vuorela is acknowledged for helpful discussions on the biology of sage. AVa, TJK and RK acknowledge the Academy of Finland (Project Nos. 218150, 125758, 255559, and 251575) and CHEMSEM graduate school for funding the study. AVe acknowledges financial support from the U.S. National Science Foundation under Grant No. CHE-1152302. JK acknowledges support from the Academy of Finland through the Centres of Excellence program and Jenny ja Antti Wihuri Foundation through Foundations' Post Doc Pool.

REFERENCES

[1] E. R. Amstalden van Hove, D. F. Smith, R. M. A. Heeren. A concise review of mass spectrometry imaging. *J. Chromatogr. A* **2010**, *1217*, 3946.
[2] A. L. Dill, L. S. Eberlin, D. R. Ifa, R. G. Cooks. Perspectives in imaging using mass spectrometry. *Chem. Commun.* **2011**, *47*, 2741.
[3] C. Wu, A. L. Dill, L. S. Eberlin, R. G. Cooks, D. R. Ifa. Mass spectrometry imaging under ambient conditions. *Mass Spectrom. Rev.* **2013**, *32*, 218.
[4] K. Schwamborn, R. M. Caprioli. Molecular imaging by mass spectrometry-looking beyond classical histology. *Nat. Rev. Cancer* **2010**, *10*, 639.
[5] B. Shrestha, J. M. Patt, A. Vertes. In situ cell-by-cell imaging and analysis of small cell populations by mass spectrometry. *Anal. Chem.* **2011**, *83*, 2947.
[6] S. G. Ostrowski, C. T. Van Bell, N. Winograd, A. G. Ewing. Mass spectrometric imaging of highly curved membranes during *Tetrahymena* mating. *Science* **2004**, *305*, 71.
[7] R. M. Caprioli, T. B. Farmer, J. Gile. Molecular imaging of biological samples: Localization of peptides and proteins using MALDI-TOF MS. *Anal. Chem.* **1997**, *69*, 4751.
[8] H. Liebl. Ion microprobe mass analyzer. *J. Appl. Phys.* **1967**, *38*, 5277.
[9] Z. Takáts, J. M. Wiseman, B. Gologan, R. G. Cooks. Mass spectrometry sampling under ambient conditions with desorption electrospray ionization. *Science* **2004**, *306*, 471.
[10] J. M. Wiseman, D. R. Ifa, Q. Song, R. G. Cooks. Tissue imaging at atmospheric pressure using desorption electrospray ionization (DESI) mass spectrometry. *Angew. Chem. Int. Ed.* **2006**, *45*, 7188.
[11] P. Nemes, A. Vertes. Laser ablation electrospray ionization for atmospheric pressure, in vivo, and imaging mass spectrometry. *Anal. Chem.* **2007**, *79*, 8098.
[12] A. Vaikkinen, B. Shrestha, T. J. Kauppila, A. Vertes, R. Kostiainen. Infrared laser ablation atmospheric pressure photoionization mass spectrometry. *Anal. Chem.* **2012**, *84*, 1630.
[13] R. K. Shori, A. A. Walston, O. M. Stafsudd, D. Fried, J. T. Walsh Jr. Quantification and modeling of the dynamic changes in the absorption coefficient of water at $\lambda = 2.94$ μm. *IEEE J. Sel. Top. Quantum Electron.* **2001**, *7*, 959.
[14] A. Vogel, V. Venugopalan. Mechanisms of pulsed laser ablation of biological tissues. *Chem. Rev.* **2003**, *103*, 577.
[15] T. J. Kauppila, T. Kuuranne, E. C. Meurer, M. N. Eberlin, T. Kotiaho, R. Kostiainen. Atmospheric pressure photoionization mass spectrometry. Ionization mechanism and the effect of solvent on the ionization of naphthalenes. *Anal. Chem.* **2002**, *74*, 5470.
[16] R. B. Cody, J. A. Laramee, H. D. Durst. Versatile new ion source for the analysis of materials in open air under ambient conditions. *Anal. Chem.* **2005**, *77*, 2297.
[17] M. Haapala, J. Pól, V. Saarela, V. Arvola, T. Kotiaho, R. A. Ketola, S. Franssila, T. J. Kauppila, R. Kostiainen. Desorption atmospheric pressure photoionization. *Anal. Chem.* **2007**, *79*, 7867.
[18] G. Morlock, Y. Ueda. New coupling of planar chromatography with direct analysis in real time mass spectrometry. *J. Chromatogr. A* **2007**, *1143*, 243.
[19] J. Pól, V. Vidová, G. Kruppa, V. Kobliha, P. Novák, K. Lemr, T. Kotiaho, R. Kostiainen, V. Havlíček, M. Volný. Automated ambient desorption-ionization platform for surface imaging integrated with a commercial Fourier transform ion cyclotron resonance mass spectrometer. *Anal. Chem.* **2009**, *81*, 8479.
[20] M. Suhaj. Spice antioxidants isolation and their antiradical activity: a review. *J. Food Compos. Anal.* **2006**, *19*, 531.
[21] K. Schwarz, W. Ternes. Antioxidative constituents of *Rosmarinus officinalis* and *Salvia officinalis*. II. Isolation of carnosic acid and formation of other phenolic diterpenes. *Z. Lebensm. Unters. Forsch.* **1992**, *195*, 99.
[22] Z. Bolta, Baričevič B. Bohanec, S. Andrenšek. A preliminary investigation of ursolic acid in cell suspension culture of *Salvia officinalis*. *Plant Cell Tissue Organ Cult.* **2000**, *62*, 57.
[23] M. I. Razboršek, D. B. Vončina, V. Doleček, E. Vončina. Determination of oleanolic, betulinic and ursolic acid in Lamiaceae and mass spectral fragmentation of their trimethylsilylated derivatives. *Chromatographia* **2008**, *67*, 433.
[24] M. Tubaro, E. Marotta, R. Seraglia, P. Traldi. Atmospheric pressure photoionization mechanisms. 2. The case of benzene and toluene. *Rapid Commun. Mass Spectrom.* **2003**, *17*, 2423.
[25] V. Saarela, M. Haapala, R. Kostiainen, T. Kotiaho, S. Franssila. Glass microfabricated nebulizer chip for mass spectrometry. *Lab Chip* **2007**, *7*, 644.
[26] P. Nemes, A. S. Woods, A. Vertes. Simultaneous imaging of small metabolites and lipids in rat brain tissues at atmospheric pressure by laser ablation electrospray ionization mass spectrometry. *Anal. Chem.* **2010**, *82*, 982.
[27] K. Schwarz, W. Ternes. Antioxidative constituents of *Rosmarinus officinalis* and *Salvia officinalis*. I. Determination of phenolic diterpenes with antioxidative activity amongst tocochromanols using HPLC. *Z. Lebensm. Unters. Forsch.* **1992**, *195*, 95.
[28] Y. Lu, L. Yeap Foo. Polyphenolics of *Salvia* – A review. *Phytochemistry* **2002**, *59*, 117.
[29] N. B. Perry, R. E. Anderson, N. J. Brennan, M. H. Douglas, A. J. Heaney, J. A. McGimpsey, B. M. Smallfield. Essential oils from Dalmatian sage (*Salvia officinalis L.*): variations among individuals, plant parts, seasons, and sites. *J. Agric. Food Chem.* **1999**, *47*, 2048.
[30] P. C. Santos-Gomes, M. Fernandes-Ferreira. Organ- and season-dependent variation in the essential oil composition of *Salvia officinalis* L. cultivated at two different sites. *J. Agric. Food Chem.* **2001**, *49*, 2908.
[31] V. Radulescu, S. Chiliment, E. Oprea. Capillary gas chromatography-mass spectrometry of volatile and semi-volatile compounds of *Salvia officinalis*. *J. Chromatogr. A* **2004**, *1027*, 121.
[32] C. Funk, A. E. Koepp, R. Croteau. Catabolism of camphor in tissue cultures and leaf disks of common sage (*Salvia officinalis*). *Arch. Biochem. Biophys.* **1992**, *294*, 306.
[33] M. Kivilompolo, V. Obůrka, T. Hyötyläinen. Comparison of GC-MS and LC-MS methods for the analysis of antioxidant phenolic acids in herbs. *Anal. Bioanal. Chem.* **2007**, *388*, 881.

[34] K. Miura, H. Kikuzaki, N. Nakatani. Apianane terpenoids from *Salvia officinalis*. *Phytochemistry* **2001**, *58*, 1171.
[35] H. Gambliel, R. Croteau. Biosynthesis of (±)-α-pinene and (–)-β-pinene from geranyl pyrophosphate by a soluble enzyme system from sage (*Salvia officinalis*). *J. Biol. Chem.* **1982**, *257*, 2335.
[36] A. Vaikkinen, B. Shrestha, J. Nazarian, R. Kostiainen, A. Vertes, T. J. Kauppila. Simultaneous detection of nonpolar and polar compounds by heat-assisted laser ablation electrospray ionization mass spectrometry. *Anal. Chem.* **2013**, *85*, 177.
[37] L. Zhu, J. Yan, Z. Zhu, Y. Ouyang, X. Zhang, W. Zhang, X. Dai, L. Luo, H. Chen. Differential analysis of camphor wood products by desorption atmospheric pressure chemical ionization mass spectrometry. *J. Agric. Food Chem.* **2013**, *61*, 547.
[38] S. D. Maleknia, T. M. Vail, R. B. Cody, D. O. Sparkman, T. L. Bell, M. A. Adams. Temperature-dependent release of volatile organic compounds of eucalypts by direct analysis in real time (DART) mass spectrometry. *Rapid Commun. Mass Spectrom.* **2009**, *23*, 2241.
[39] V. Kertesz, G. J. Van Berkel. Improved imaging resolution in desorption electrospray ionization mass spectrometry. *Rapid Commun. Mass Spectrom.* **2008**, *22*, 2639.
[40] D. I. Campbell, C. R. Ferreira, L. S. Eberlin, R. G. Cooks. Improved spatial resolution in the imaging of biological tissue using desorption electrospray ionization. *Anal. Bioanal. Chem.* **2012**, *404*, 389.
[41] A. Bisio, A. Corallo, P. Gastaldo, G. Romussi, G. Ciarallo, N. Fontana, N. De Tommasi, P. Profumo. Glandular hairs and secreted material in *Salvia blepharophylla* Brandegee ex Epling grown in Italy. *Ann. Bot.* **1999**, *83*, 441.
[42] R. Croteau, F. Karp. Demonstration of a cyclic pyrophosphate intermediate in the enzymic conversion of neryl pyrophosphate to borneol. *Arch. Biochem. Biophys.* **1977**, *184*, 77.
[43] R. Croteau, M. Felton, F. Karp, R. Kjonaas. Relationship of camphor biosynthesis to leaf development in sage (*Salvia officinalis*). *Plant Physiol.* **1981**, *67*, 820.
[44] I. Bettaieb, N. Zakhama, W. A. Wannes, M. E. Kchouk, B. Marzouk. Water deficit effects on *Salvia officinalis* fatty acids and essential oils composition. *Sci. Hortic.* **2009**, *120*, 271.

SUPPORTING INFORMATION

Additional supporting information may be found in the online version of this article at the publisher's website.

Supporting Information

Laser Ablation Atmospheric Pressure Photoionization Mass Spectrometry Imaging of Phytochemicals from Sage Leaves

Anu Vaikkinen,[a] Bindesh Shrestha,[b] Juha Koivisto,[c] Risto Kostiainen,[a] Akos Vertes[b*] and Tiina J. Kauppila[a*]

[a] *Division of Pharmaceutical Chemistry and Technology, Faculty of Pharmacy, P.O. Box 56, 00014 University of Helsinki, Finland*
[b] *Department of Chemistry, W. M. Keck Institute for Proteomics Technology and Applications, George Washington University, Washington, DC 20052, USA*
[c] *Department of Physics and Astronomy, University of Pennsylvania, Philadelphia, PA 19104, USA*

Corresponding Authors

Tiina J. Kauppila
Division of Pharmaceutical Chemistry and Technology
Faculty of Pharmacy, University of Helsinki
P.O. Box 56 (Viikinkaari 5 E)
00014 University of Helsinki
Helsinki, Finland
Phone: +358 2941 59169
Fax: +358 2941 59556
E-mail: tiina.kauppila@helsinki.fi

Akos Vertes
Department of Chemistry
W. M. Keck Institute for Proteomics Technology and Applications
George Washington University
Washington DC 20052, United States
Phone: +1 (202) 994-2717
Fax: +1 (202) 994-5873
E-mail: vertes@gwu.edu

SCRIPT FOR PRODUCING THE MS IMAGES

The algorithms are written with Python programming language utilizing version 2.7 and corresponding numpy, scipy and matplotlib libraries. The goal of the first function is to combine the time-location and time-intensity data and to create location-intensity maps (getIntensityMap). The second function (getColocalizationMap) calculates the Pearson colocalization maps. The rest of the functions are for plotting and for visualizing the data in a meaningful way. Sample images are given below.

```
import numpy
import pylab
import matplotlib

def getIntensityMap(jmcFn, timeFn, gridShape = (22,51)):
    """
    Combine time-intensity data to x-y-time data. TimeFn contains
    the times when spot xy is exposed to ablation. jmcFn contains
    the time intensity data (1 Hz). The output is the integrated
    intensity iMap at positions xMap,yMap. The algorithm
    integrates from the time the spot is exposed to ablation until
    a) 5 data points are read or b) the next spot is exposed,
    whichever is shorter.

    inputs

    jmcFn     : Time-intensity data filename produced by mass
                spectrometer software
                Two columns: time and intensity.
    timeFn    : X-y-time data filename produced by xy-stage
                software.
                Three columns: x, y and entry time.
    gridShape : Number of (horizontal, vertical) spots.


    outputs

    xMap      : 2D array of x-coordinates
    yMap      : 2D array of y-coordinates
    iMap      : 2D array of integrated intensities

    usage:

    from intensityMap import getIntensityMap
    import pylab
    xMap, yMap, iMap = getIntensityMap('EIC 136.jmc',
                                       'salvia time.txt')
    iMap[iMap > 20000] = 20000     # threshold
    pylab.contourf(xMap, yMap, iMap)
    pylab.show()
    """

    # load time-intensity to array
    ti = numpy.loadtxt(jmcFn)
    # load x-y-time to array
```

```
    xyt = numpy.loadtxt(timeFn)

    # create time and intensity vectors
    t_i = ti[:,0]
    i_i = ti[:,1]

    # create x,y and time intensity vectors
    x_xy = xyt[:,0]
    y_xy = xyt[:,1]
    t_xy = xyt[:,2]

    # create vectors for output
    xMap = []
    yMap = []
    iMap = []

    # create index vector for convenience
    indexVector = numpy.arange(len(t_i))

    # loop through all spot times
    for i in range(len(t_xy)):

        # get time intervals corresponding to current spot
        startTime = t_xy[i]
        try:
            endTime = t_xy[i+1]
        except: # last point is missing, extrapolate end time
            step = t_xy[i] - t_xy[i-1]
            endTime = startTime + step

        # get indices corresponding to start and end time
        minIndex = numpy.min(indexVector[t_i >= startTime])
        maxIndex1 = numpy.min(indexVector[t_i >= endTime])

        # apply "max 5 points" restriction
        maxIndex2 = minIndex + 5
        maxIndex = numpy.min([maxIndex1, maxIndex2])

        # integrate over possibly variable length vector
        intensityVector = i_i[minIndex:maxIndex]
        intensity = numpy.mean(intensityVector)*5

        # put results to vectors
        xMap.append(x_xy[i])
        yMap.append(y_xy[i])
        iMap.append(intensity)

    # reshape to 2D numpy array
    xMap = numpy.array(xMap).reshape(gridShape)
    yMap = numpy.array(yMap).reshape(gridShape)
    iMap = numpy.array(iMap).reshape(gridShape)

    return xMap, yMap, iMap

def getColocalizationMap(iMap1, iMap2):
    """
    Calculates pearson colocalization map from N dimension intensity maps.
```

```
    The intensity maps are assumed to have the same spatial coordinates.

    iMap1, iMap2    : intensity maps produced by e.g. getIntensityMap
                      function. same shape is assumed.
    returns         : Pearsons correlation map with the same shape as
                      iMap1 and iMap2
    """

    ave1Rem = (iMap1 - numpy.mean(iMap1))
    ave2Rem = (iMap2 - numpy.mean(iMap2))
    std1 = numpy.std(iMap1)
    std2 = numpy.std(iMap2)

    return ave1Rem*ave2Rem/(std1*std2)

def plotIntensityMap(xMap, yMap, iMap,
                     threshold = 32000,
                     xShift = -2,
                     yShift = -2,
                     contourStep = 0.02,
                     colorTickValues = [0,25,50,75]):
    """
    Plots intensity map relative to maximum intensity (i.e. intensity in
    procents). Values higher than <threshold> are cut away.
    Spatical locations are shifted by <xShift> and <yShift>. Contourlines
    are with spacing of <contourStep> and contourlabels are in procent
    indicated by <colorTickValues>. Also, the maximum relative intensity is
    shown if the threshold cuts the peaks. Runs tweakPlot at the end for
    nice visualization.

    xMap              : 2D array of x-coordinates
    yMap              : 2D array of y-coordinates
    iMap              : 2D array of integrated intensities
    threshold         : cut peaks if hihgher than this (absolute values)
    xShift            : shift x-coordinate (for pretty output)
    yShift            : shift y-coordinate (for pretty output)
    contourStep       : step between contourlines
    contourTickValues : values shown in colorbar
    """

    # apply threshold
    maxIntensity = numpy.max(iMap)
    if threshold:
        iMap[iMap > threshold] = threshold

    # scale to 100 %
    iMap = iMap * 100.0/maxIntensity

    contourVector = numpy.arange(numpy.min(colorTickValues),
                                 numpy.max(iMap) + contourStep,
                                 contourStep)
    im=pylab.contourf(xMap+xShift, yMap+yShift, iMap,
                      contourVector)

    # color tick values
    #ctv = [numpy.min(iMap)]
    ctv = colorTickValues
```

```
    ctv += [numpy.max(iMap)]

    # color tick labels
    ctl = []
    for value in ctv:
        ctl.append("%d %%" % (value))
    if ctv[-1] < 99.9:
        ctl[-1] = "> %d %%" % (numpy.round(ctv[-1]))

    # make it look nice
    tweakPlot(im, ctv, ctl)

def plotPearsonCorrelationMap(xMap, yMap, pMap, logColor=True,
                              lowerThres = 0.07, xShift = -2, yShift = -2):

    # remove small values (noise)
    pMap[pMap < lowerThres] = lowerThres

    # suppress peaks by log (or not)
    if logColor:
        pMap = numpy.log(pMap)

    # create colorLabels and values
    cbarValues = numpy.arange(numpy.min(pMap), numpy.max(pMap))
    if logColor:
        cbarLabels = numpy.round(numpy.exp(cbarValues),2)
    else:
        cbarLabels = numpy.round(cbarValues,2)

    # plot contourplot
    im = pylab.contourf(xMap+xShift, yMap+yShift, pMap, 100,
                        cmap = matplotlib.cm.bone)

    # make it look nice
    tweakPlot(im, cbarValues, cbarLabels)


def tweakPlot(image, colorbarvalues, colorbarlabels, fontsize = 15):
    """
    Tweaks plot: colorbars, labels, fontsizes, positions, etc.
    Operates on current figure: pylab.gcf() and axis: pylab.gca().

    image             : contourplot image to which colorbar is attached
    colorbarvalues    : array of values where to put colorbar labels
    colorbarlabels    : array of strings (or floats) of corresponding
                        to <colorbarvalues>
    """

    # tweak axis
    ax = pylab.gca()
    ax.invert_xaxis()
    ax.set_aspect('equal')

    # tweak labels
    pylab.xlabel('x (mm)', fontsize= fontsize)
    pylab.ylabel('y (mm)', fontsize= fontsize)
    for label in ax.get_xticklabels() + ax.get_yticklabels():
```

```
        label.set_fontsize(fontsize)

    pylab.subplots_adjust(left=0.1, right=0.78, top=0.9, bottom=0.1)

    # tweak colorbar
    fig = pylab.gcf()
    axcb = fig.add_axes([.8, 0.17, 0.02, .65])

    cb = fig.colorbar(image, cax=axcb, extend='both')
    cb.set_ticks(colorbarvalues)
    try:
        axcb.set_yticklabels(numpy.round(colorbarlabels,2))
    except:
        axcb.set_yticklabels(colorbarlabels)

    for label in axcb.get_xticklabels() + axcb.get_yticklabels():
        label.set_fontsize(fontsize)
        label.set_ha('left')
        pos = label.get_position()
        label.set_position((pos[0] + 0, pos[1]))

if __name__ == "__main__":

    # Figure 1, intensity map of mass 136
    pylab.figure(1, figsize=(12, 5))
    xMap, yMap, iMap = getIntensityMap('EIC 136.jmc',
                                       'salvia time.txt')

    plotIntensityMap(xMap, yMap, iMap)
    pylab.savefig('exampleIntensity.png')

    # Figure 2, pearson correlation map for masses 136 and 153
    pylab.figure(2, figsize=(12, 5))
    xMap2, yMap2, iMap2 = getIntensityMap('EIC 153.jmc',
                                          'salvia time.txt')
    pMap = getColocalizationMap(iMap2, iMap)
    plotPearsonCorrelationMap(xMap, yMap, pMap)
    pylab.savefig('exampleCorrelation.png')

    pylab.show()
```

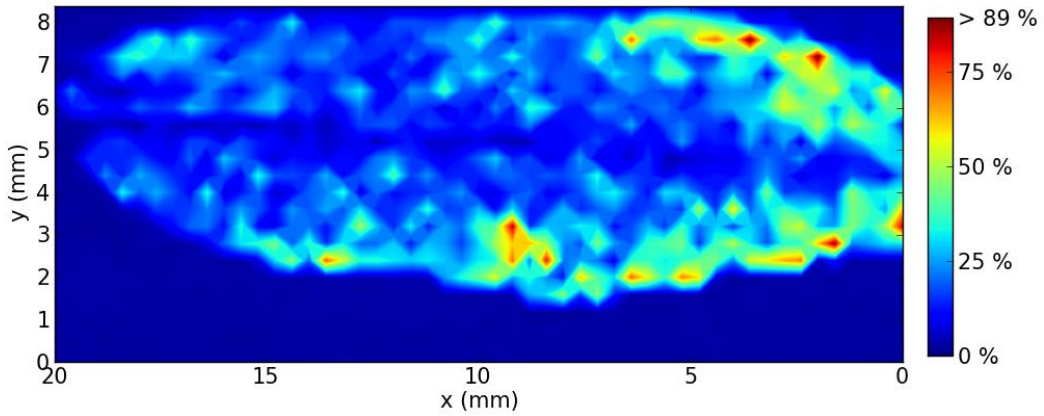

Example 1. Distribution of *m/z* 136.14 signal from sage leaf with intensity threshold at 89 % (see also Figure 3c of the main text).

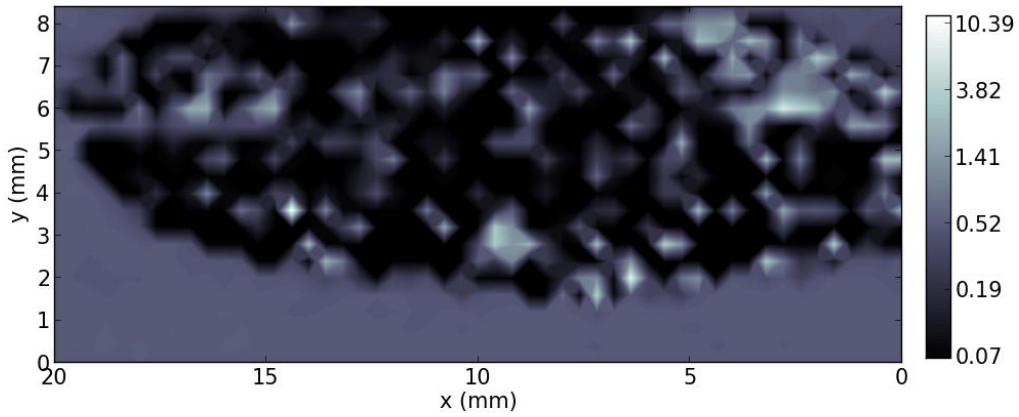

Example 2. Colocalization of ions at *m/z* 136.14 and 456.35 in the sage leaf.

CORRELATION AND COLOCALIZATION ANALYSIS

Correlation analysis of the ion intensities was performed to investigate whether the observed ions could have been produced by fragmentation or oxidation from other species. It was assumed that localized biological conversions could be distinguished from those occurring due to exposure to air or during ionization, because the latter are repeatable and independent of the location and thus result in high correlation of the respective ion abundances. The analysis was similar to that reported previously for LAESI-MSI. [1, 2]

The correlation analysis was performed by plotting the intensities of two ions of interest at each recorded data point against each other using OriginPro 8.6.0 (OriginLab Corporation, Northampton, MA, USA). Note that in addition to the MS image data, the analysis also included data for sample transfer/wait times between the rows, which resulted in additional data not included in the images. A scatter plot of the intensity values was obtained for each pair of ions. The scatter plots were visually inspected and subjected to linear regression analysis. The obtained values of Pearson's *r* (Pearson product-moment cross correlation coefficients) of the linear fit were considered as the quantitative indicator for the correlation of the spatial distributions of the two ions. Figure S1 shows representative scatter plots of selected ion pairs and Table S1 gives an overview of the obtained Pearson's *r* values. Tables S2-4 present additional correlation matrices for the highly correlated ion groups that are reported in Table 1. Note that only the ions observed from the sage leaves and listed in Table 1 were subjected to the correlation analysis. Therefore negative (linear) correlation was not found for any of the studied ion pairs. However, virtually no correlation was found for some of the studied ion pairs (Pearson's $r \leq 0.500$) and these are highlighted using blue in Tables S1-4, while the pairs with high correlation (Pearson's $r \geq 0.975$) are highlighted using yellow.

The correlation analysis showed that, e.g., the ion at *m/z* 286.19 is probably the fragmentation product of a diterpene ($M^{+\cdot}$ at *m/z* 332.19), possibly carnosic acid, while the ion at *m/z* 248.18 is probably a fragment of the ion(s) at *m/z* 456.35, 455.35 or 439.35. In addition, possible products of rapid air or photo-oxidation were detected, e.g., in the case of the ion at *m/z* 316.20 that could be due to the oxidation of the species at *m/*z 300.20.

For the colocalization analysis, Pearson colocalization maps were created by calculating $M_{ij}(x,y)= (I_i(x,y) - \langle I_i \rangle)(I_j(x,y) - \langle I_j \rangle)/(\sigma_i\sigma_j)$ (where $I_i(x,y)$ is the intensity of ion *i* at position (*x*,*y*), $\langle I_i \rangle$ is the average of the *i* ion intensities in the image, and σ_i is their standard deviation) for each sampled spot, and plotting the values in 2D format using a custom-written algorithm described above. Similar analyses had been presented for, e.g., LAESI-MSI data.[1, 2]

[1] P. Nemes, A. S. Woods, A. Vertes. *Anal. Chem.* **2010**, *82*, 982.

[2] P. Nemes, A. A. Barton, A. Vertes. *Anal. Chem.* **2009**, *81*, 6668.

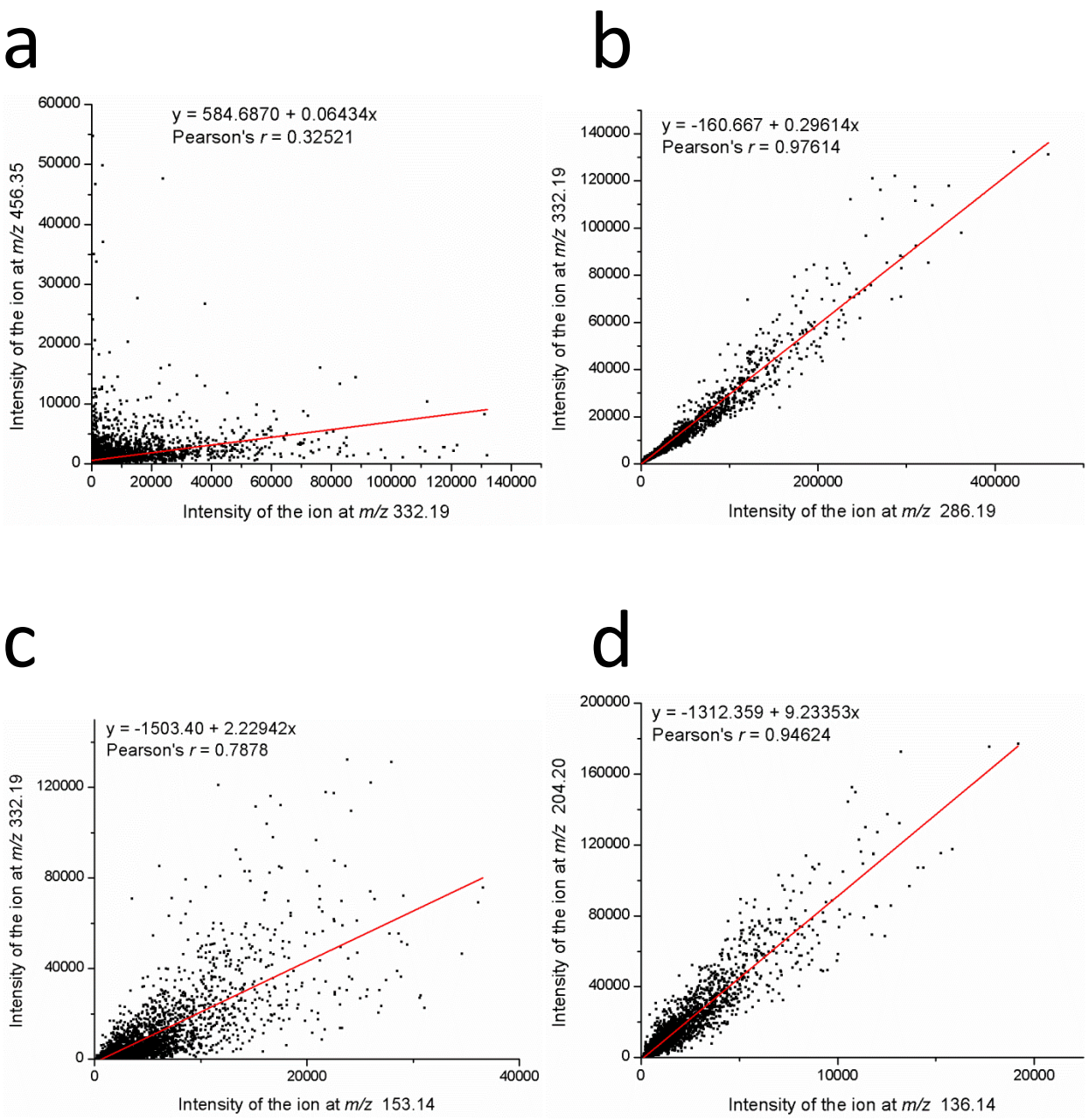

Figure S1. A scatter plot of the spatially resolved intensities of the ions at *m/z* a) 456.35 *vs* 332.19, b) 332.19 *vs* 286.19, c) 332.19 *vs* 153.14, and d) 204.20 *vs* 136.14 in sage leaves. The high correlation of the intensity of the ions in b) was thought to be due to the loss of CO and H_2O from the ion at *m/z* 332.19 to produce the ion at *m/z* 286.19. The lower but still clear correlation in d) can be explained by the storage of sesqui- (*m/z* 204.20) and monoterpenes (*m/z* 136.14) in similar secretory sites.

Table S1. Correlation matrix for selected ion pairs studied by LAAPPI-MSI. Blue background indicates a lack of correlation, and yellow represents highly correlated ion pairs. The matrix components were chosen to include abundant ions over the range of *m/z* 100-550, including all those with MSI images shown in Figure 3 of the main text, as well as those of correlation groups 4 and 7 reported in Table 1.

Pearson's *r*		*m/z*																
		136.07	136.14	153.14	155.15	167.12	169.13	204.20	219.17	237.19	248.18	286.19	300.20	316.20	332.19	346.21	439.35	456.35
m/z	136.07	1																
	136.14	0.41413	1															
	153.14	0.34407	0.86112	1														
	155.15	0.28159	0.93214	0.90775	1													
	167.12	0.36808	0.83737	0.87826	0.84084	1												
	169.13	0.32308	0.91495	0.89957	0.92427	0.96226	1											
	204.20	0.34267	0.94624	0.86906	0.89627	0.79677	0.86714	1										
	219.17	0.3838	0.91886	0.8948	0.89423	0.87549	0.91269	0.96332	1									
	237.19	0.37357	0.92118	0.89384	0.89765	0.90745	0.93825	0.94663	0.97514	1								
	248.18	0.38022	0.32988	0.33953	0.27123	0.3037	0.29173	0.39145	0.47976	0.34568	1							
	286.19	0.33673	0.85828	0.81743	0.80746	0.75374	0.80969	0.92326	0.89458	0.89867	0.35461	1						
	300.20	0.36873	0.78144	0.7479	0.72106	0.67771	0.71445	0.86228	0.82934	0.84702	0.34049	0.95308	1					
	316.20	0.40214	0.75956	0.7245	0.69514	0.67082	0.69999	0.82526	0.7962	0.82411	0.32517	0.91701	0.97889	1				
	332.19	0.30056	0.85844	0.7878	0.81000	0.73289	0.80509	0.92099	0.87964	0.88435	0.33085	0.97614	0.92339	0.89171	1			
	346.21	0.3154	0.84809	0.79578	0.79594	0.73958	0.79672	0.92267	0.89111	0.89021	0.35388	0.97607	0.95136	0.91336	0.98412	1		
	439.35	0.41582	0.33081	0.34323	0.27258	0.30624	0.28865	0.38855	0.48058	0.34718	0.97919	0.34982	0.34406	0.3311	0.32295	0.34708	1	
	456.35	0.37911	0.32741	0.34715	0.27517	0.30989	0.29331	0.38753	0.47882	0.34718	0.98611	0.34966	0.3417	0.32921	0.32521	0.349	0.98632	1

Table S2. Correlation matrix for selected ions from sage leaves studied by LAAPPI-MSI (correlation groups 1-3 in Table 1).

Pearson's *r*		*m/z*				
		133.12	147.13	189.17	203.19	204.20
m/z	133.12	1				
	147.13	0.86417	1			
	189.17	0.97265	0.93832	1		
	203.19	0.9769	0.88638	0.98048	1	
	204.20	0.90278	0.98189	0.95484	0.9242	1

Table S3. Correlation matrix for selected highly correlated ions from sage leaves studied by LAAPPI-MSI (correlation group 6 in Table 1).

Pearson's *r*		*m/z*			
		286.19	331.19	332.19	346.21
m/z	286.19	1			
	331.19	0.9788	1		
	332.19	0.97614	0.97814	1	
	346.21	0.97607	0.98266	0.98412	1

Table S4. Correlation matrix for selected highly correlated ions from sage leaves studied by LAAPPI-MSI (correlation group 5 in Table 1).

Pearson's *r*		*m/z*				
		248.18	437.34	439.35	455.35	456.35
m/z	248.18	1				
	437.34	0.96883	1			
	439.35	0.97919	0.97788	1		
	455.35	0.97524	0.99098	0.98122	1	
	456.35	0.98611	0.99006	0.98632	0.99178	1